Onset of convection in a porous medium in the presence of chemical reaction

Jeanne Therese H. Andres and Silvana S. S. Cardoso*

Department of Chemical Engineering & Biotechnology, University of Cambridge, Cambridge CB2 3RA, United Kingdom

(Received 26 September 2010; revised manuscript received 14 February 2011; published 22 April 2011)

Using scaling, we show that the stability of a buoyant boundary layer in a porous medium in the presence of a first-order chemical reaction is fully determined by the nondimensional number $\mathrm{Da}/\mathrm{Ra}^2 = k_r a D\phi\mu^2/(k\Delta\rho_0 g)^2$, where $\mathrm{Da} = k_r a L_Z^2/(D\phi)$ is the Damköhler number and $\mathrm{Ra} = k\Delta\rho_0 g L_Z/(\mu D\phi)$ is the solutal Rayleigh number. The time for onset of convection is shown to increase with rising $\mathrm{Da}/\mathrm{Ra}^2$. Above a critical $\mathrm{Da}/\mathrm{Ra}^2 \approx 2\times 10^{-3}$, no convection occurs as reaction stabilizes the diffusive layer at a finite thickness. This thickness decreases with increasing $\mathrm{Da}/\mathrm{Ra}^2$, becoming zero at $\mathrm{Da}/\mathrm{Ra}^2 \approx \mathrm{O}(1)$. As applied to CO_2 geostorage, our results suggest distinct regimes for CO_2 transport in saline aquifers.

DOI: 10.1103/PhysRevE.83.046312 PACS number(s): 47.20.Bp, 47.56.+r, 47.70.Fw, 82.33.Ln

I. INTRODUCTION

The behavior of buoyancy-driven flows in porous media has relevance in fields as diverse as petroleum and environmental engineering, ground water hydrology, geophysics, and biomedical engineering. When a fluid in a porous medium is heated from below, a thermal boundary layer of less dense, hot fluid develops and grows with time. This boundary layer eventually becomes unstable and breaks up, driving bulk convection in the fluid above. Horton and Rogers [1] and Lapwood [2] independently proposed a critical Rayleigh number, $\mathrm{Ra}_C = 4\pi^2$, as a criterion for the onset of such natural convection in a porous medium. This theory was later confirmed by experimental results [3].

In recent years, more complex flows with chemical reaction have considered the effects of reaction kinetics at a fluid interface or boundary. Interfacial reactions have been revealed to prevent the elongation of a moving chemical front at large times, thus yielding dispersion curves independent of time, and finger growth rates which are smaller than the initial growth rate of density-dependent instabilities in the absence of reaction [4,5]. The interaction between diffusion and reaction at an interface has been found to induce convection in an otherwise stably stratified system, as well as affect the formation of symmetric patterns in buoyantly unstable systems [6]. Numerical work on the onset of convection in a system where thermal convection is driven by an exothermic surface reaction on the bottom boundary suggests that Ra_C is affected by the Lewis number, based on the diffusivity of the reactant, as well as the nondimensional reaction rate [7].

Others have investigated natural convection arising from heat generated by a chemical reaction occurring throughout the bulk fluid in a porous medium. In a problem formulated in Ref. [8], convection following the Darcy-Boussinesq model is driven by a zero-order exothermic reaction taking place in a cylinder filled with porous material. Their numerical results showed that this chemically driven convection increased critical thermal ignition temperatures, and is capable of delaying or averting thermal ignition when the Rayleigh number is sufficiently large. The bifurcation and stability behavior of a similar, but simplified, system was studied numerically for a two-dimensional rectangular geometry [9], while the authors of Ref. [10] performed a stability analysis for similar reaction-driven convection in both cylindrical and three-dimensional rectangular geometries. Stability analysis of an inert horizontal porous layer where thermal convection develops due to cooling from the top, as well as from a weakly exothermic zero-order gas-phase reaction, found that Ra_C decreases with increasing values of the Frank-Kamenetskii number, thus showing that instability is enhanced by the presence of such reactions, in comparison with cases in which reactions do not occur [11].

In this work, we examine the effect of a first-order chemical reaction on the stability of a buoyant diffusive boundary layer in a porous medium. We identify conditions for which even a simple chemical reaction may significantly delay or inhibit the breakdown of the boundary layer and the onset of natural convection in the underlying bulk fluid. Using scaling, we show that the basic interaction between fluid flow and chemical kinetics is governed by a ratio of the well-known Damköhler and Rayleigh numbers. We also determine the time for onset of convection in a reactive medium as a function of the new dimensionless number.

II. MODEL SYSTEM

A. Geological CO_2 sequestration

The principal motivation for this study has been to understand the behavior of CO_2 stored in deep saline aquifers [12]. Determining the onset of natural convection in subsurface CO_2-brine systems is crucial to establish definite time scales for potential leakage scenarios, complete CO_2 dissolution, and long-term mineral dissolution and precipitation. Figure 1 depicts the problem in the context of CO_2 sequestration. Upon injection into a saline reservoir, supercritical CO_2, being less dense than aquifer brine, rises and spreads laterally under an impermeable cap rock. Some of this CO_2 dissolves in the brine below it, causing a small density increase which may eventually cause instability in the diffusive boundary layer. This instability drives convection in the fluid below and accelerates further dissolution as the CO_2-rich brine sinks and is transported away from the interface [13,14]. By increasing CO_2 mass transfer rates into the brine, convection shortens the time needed to completely dissolve the CO_2 [13,15]. Convection also enhances contact between dissolved CO_2

*sssc1@cam.ac.uk

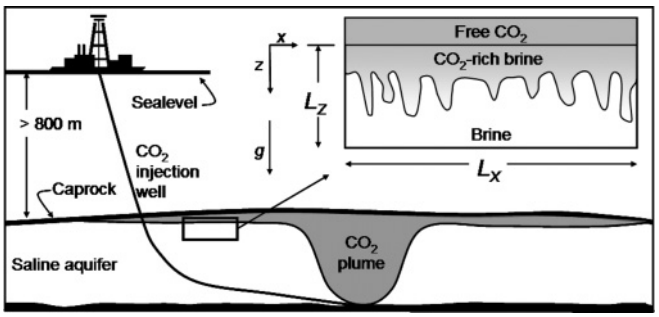

FIG. 1. Injected CO_2 (shaded) rises in a brine-saturated aquifer and spreads laterally under a caprock. Inset: Free CO_2 (shaded) gradually dissolves and diffuses in the underlying brine, resulting in a denser CO_2-rich solution (shaded gradient) which may later sink into the pure brine as fingers, enhancing further dissolution.

and rock minerals as they react to form ionic species and precipitates, thus facilitating permanent CO_2 sequestration. It has been suggested that fast chemical reactions may increase the time for onset of convective mixing [16], but such an effect has not been quantified in a general manner.

B. Governing equations

We consider a two-dimensional homogeneous, isotropic porous medium with dimensions and orientation as shown in the inset of Fig. 1. A simple A→B reaction occurs between a dissolved species (aqueous CO_2) and a chemical species in the porous matrix (rock), with reaction rate $k_r a[T^{-1}]$ per unit volume of fluid, where the solid-based kinetic rate constant is $k_r[\mathrm{mol}\,L^{-2}T^{-1}]$ and the reactive surface area per mole of the solid is $a[L^2\,\mathrm{mol}^{-1}]$. The system may be described by the continuity equation (1) and Darcy's law (2) for the fluid transport velocity $\mathbf{v}[LT^{-1}]$, coupled with the conservation of dissolved species (3) with concentration $C[ML^{-3}]$:

$$\nabla\cdot\mathbf{v}=0, \tag{1}$$

$$\mathbf{v}=-\frac{k}{\mu}(\nabla p-\rho_r\beta C g\mathbf{i}), \tag{2}$$

$$D\phi\,\nabla^2 C-\mathbf{v}\cdot\nabla C=\phi\frac{\partial C}{\partial t}+k_r a C. \tag{3}$$

Density changes are assumed to be small [17] and therefore neglected except in the buoyancy term in (2) under the Oberbeck-Boussinesq approximation [18]. The permeability of the porous medium $k[L^2]$ and the fluid viscosity $\mu[ML^{-1}T^{-1}]$ are constant, while the reduced pressure $p=P-\rho_r g z[ML^{-1}T^{-2}]$ is obtained by eliminating the hydrostatic pressure from $P[ML^{-1}T^{-2}]$, the pressure in the liquid. We assume the density $\rho[ML^{-3}]$ to depend linearly on C as $\rho=\rho_r(1+\beta C)$, where the reference density $\rho_r[ML^{-3}]$ and the coefficient of density change due to concentration $\beta[-]$ are constant. The acceleration due to gravity is $g[LT^{-2}]$ and $\mathbf{i}$ is a vertical unit vector codirectional with the positive z axis. In systems where diffusion dominates over convective dispersion and where tortuosity is low, the effective diffusivity of the dissolved species in the porous medium is simply taken as the product of the molecular diffusion coefficient $D[L^2T^{-1}]$ of CO_2 in the brine and the porosity $\phi[-]$ of the aquifer. Time is denoted by $t[T]$.

At $t=0$, the entire domain is quiescent and CO_2 free, i.e., $\forall x,\ \forall z:\mathbf{v}=0,\ C=0$. Boundary conditions are $v_X=0$ and $\partial C/\partial x=0$ at the walls ($x=0$ and $x=L_X$), and $v_Z=0$ and $\partial C/\partial z=0$ at the bottom ($z=L_Z$), where v_X and v_Z are the respective horizontal and vertical components of $\mathbf{v}$. The top boundary of the system ($z=0$) is then instantaneously exposed to an overlying layer of free CO_2, expressed by the boundary condition $C(x,0,t)=C_s$, where C_s is the solubility of CO_2 in brine [13,14]. Although there is a small downward flux of CO_2 at the top boundary, the associated fluid vertical velocity is very small and has been shown to be negligible for low solubility and concentration values, such as those for a CO_2 system [17].

C. Nondimensionalization

We note that the reservoir bottom boundary, and hence vertical extent L_Z, has no effect on the initial development of convection in the top layer of diffusing CO_2. This allows us to use an internal length scale for the problem. We chose the convective length scale $L_C=\mu D\phi/(k\Delta\rho_0 g)$, which is a measure of the thickness of the boundary layer at the time of instability, i.e., when the inhibiting effects of diffusion and reaction balance the driving effect of buoyancy on the development of fluid motion, making the solutal Rayleigh number of order unity. Thus, when $L_Z/L_C\gg 1$, we expect the onset of convection to be independent of the vertical extent of the reservoir. This approach has been used previously by Refs. [17] and [19] for inert systems.

Equations (1)–(3) are nondimensionalized using the scales L_C, $v_s=D\phi/L_C$, $t_s=L_C^2/D$, $p_s=\mu D\phi/k$, and C_s, giving

$$\nabla'\cdot\mathbf{v}'=0, \tag{4}$$

$$\mathbf{v}'=-\nabla' p'+C'\mathbf{i}, \tag{5}$$

and

$$\nabla'^2 C'-\mathbf{v}'\cdot\nabla' C'=\frac{\partial C'}{\partial t'}+\frac{\mathrm{Da}}{\mathrm{Ra}^2}C'. \tag{6}$$

The initial conditions become $\mathbf{v}'(x',z',0)=0$ and $C'(x',z',0)=0$, and the boundary conditions become $v'_X=0$ and $\partial C'/\partial x'=0$ at the walls ($x'=0$ and $x'=L_X/L_C$), $v'_Z=0$ and $\partial C'/\partial z'=0$ at the bottom ($z'=L_Z/L_C$), and $v'_Z=0$ and $C'=1$ at the top ($z'=0$). Here, $\mathrm{Ra}=k\Delta\rho_0 g L_Z/(\mu D\phi)$ is the solutal Rayleigh number, where $\Delta\rho_0=\rho_r\beta C_S$ is the maximum density contrast between pure and CO_2-saturated brine, and $\mathrm{Da}=k_r a L_Z^2/(D\phi)$ is the Damköhler number. We have used here the vertical extent of the reservoir L_Z to calculate individual nominal values of Ra and Da, as this will enable easier quantification and comparison with previous investigations.

From the above analysis, it is clearly evident that the only parameter determining flow and transport in this system is

$$\frac{\mathrm{Da}}{\mathrm{Ra}^2}=\frac{k_r a D\phi}{(k\Delta\rho_0 g/\mu)^2}, \tag{7}$$

when the penetration depth of the CO_2-rich layer is smaller than the reservoir depth. The CO_2 mass flux $J[ML^{-2}T^{-1}]$ dissolving at the top boundary is given by $J=(D\phi/L_X)\int_0^{L_X}(dC/dz)dx$ or, in dimensionless form, $J'=JL_C/(D\phi C_S)$.

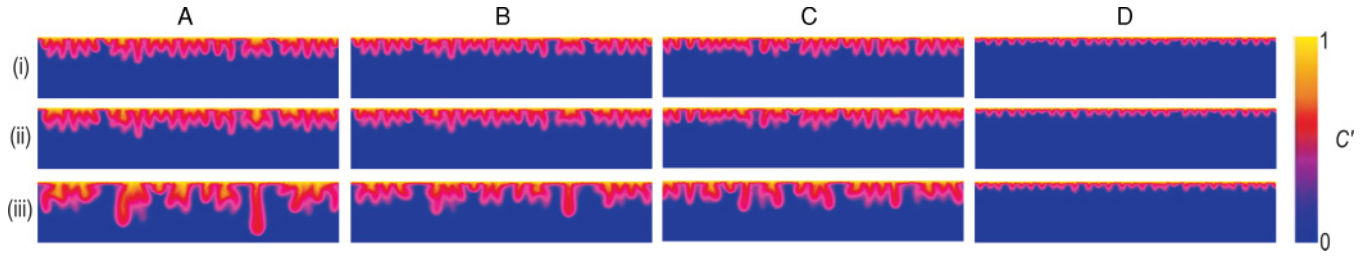

FIG. 2. (Color online) Effects of Da/Ra^2 on dimensionless CO_2 concentration C' at dimensionless times (i) $t' = 3.3 \times 10^3$, (ii) $t' = 3.8 \times 10^3$, and (iii) $t' = 5.7 \times 10^3$. Inert case A ($Da = 0$, $Ra = 750$, $Da/Ra^2 = 0$) shows a faster growth rate of CO_2-rich fingers than in reactive cases B ($Da = 86$, $Ra = 750$, $Da/Ra^2 = 1.5 \times 10^{-4}$), C ($Da = 345$, $Ra = 1500$, $Da/Ra^2 = 1.5 \times 10^{-4}$) and D ($Da = 571$, $Ra = 750$, $Da/Ra^2 = 1 \times 10^{-3}$). Significant finger interaction is seen in A, B, and C, where larger merged fingers grow deeper, while reaction in D is strong enough to inhibit growth of merged fingers, stabilizing their lengths at a constant depth. Dimensionless wavelength at onset of instability is similar in all four cases. Each picture shows half of the domain width used in simulations, and pictures of C show only the active, upper half of the simulated depth.

D. Numerical simulations

The governing partial differential equations (1)–(3), together with corresponding initial and boundary conditions, were solved numerically using the finite-element partial differential equation (PDE) solver FASTFLO [20]. The numerical algorithm employs Picard's method of successive approximations, a backward Euler time-stepping scheme, and the augmented Lagrangian method [20]. The coupled momentum and continuity equations were solved iteratively within each time step m until $\mathbf{v}$ and p met two convergence criteria. The first criterion required that the relative velocity change between consecutive iterations n and $n-1$, summed over all mesh nodes, be $\varepsilon_1 = \sum |\mathbf{v}_{m,n} - \mathbf{v}_{m,n-1}| / \sum |\mathbf{v}_{m,n}| \leqslant 0.05$. The second ensured that the maximum acceptable dimensionless velocity divergence $\nabla' \cdot \mathbf{v}'$ between iterations was $\varepsilon_2' = 5 \times 10^{-4}$, thus satisfying continuity. With a dimensionless time step $2.83 \leqslant \Delta t' \leqslant 7.54$, the coupled continuity and momentum equations typically achieved convergence within two iterations.

Tests were conducted to ensure that numerical results were independent of mesh size and time-step interval. A rectangular mesh of six-noded triangular elements was used for each simulation. Simulations were run with meshes of 5710, 7710, 9454, 11 454, 13 422, and 15 678 triangular elements. Results were deemed mesh independent when the relative difference in local concentration values between successive mesh resolutions fell below 2%. The minimum number of required elements for convergence decreased weakly with Da and, in general, increased with Ra. For $Ra = 750$, mesh independence was achieved for a minimum of 7710 elements; for higher Ra, 9454 elements were usually sufficient, except when the aspect ratio (L_X/L_Z) was halved, in which case mesh independence required 15 678 elements for $Ra = 1500$. Regular time-step intervals were varied for inert cases, starting with $2.83 \times 10^2 \leqslant \Delta t' \leqslant 7.54 \times 10^2$ and decreasing this by 50% in subsequent runs. Results were found to be independent of time-step interval at $2.83 \leqslant \Delta t' \leqslant 7.54$.

The numerical algorithm was further validated against salt-convection analogues of the Elder "short-heater problem" [21–23], widely used as a benchmark for density-driven flow simulations.

Simulations were run for the range $0 < Da/Ra^2 < 70$, with $0 < Da < 4 \times 10^7$ and $750 < Ra < 2000$. Typically, $L_Z/L_C \geqslant 750$ and $L_X/L_C \geqslant 7500$, so that the effects of the bottom and side boundaries on the onset of convection can be neglected.

III. SIGNIFICANCE OF Da/Ra^2 ON THE DEVELOPMENT OF INSTABILITY

A. Growth rate and initial wavelength of fingers

The effects of Da/Ra^2 on the development of gravitational instability are illustrated in Fig. 2. Upon comparing a chemically inert case A ($Da = 0$, $Ra = 750$, $Da/Ra^2 = 0$) with a weakly reactive case B ($Da = 86$, $Ra = 750$, $Da/Ra^2 = 1.5 \times 10^{-4}$), a reactive but more convective case C ($Da = 345$, $Ra = 1500$, $Da/Ra^2 = 1.5 \times 10^{-4}$), and case D ($Da = 571$, $Ra = 750$, $Da/Ra^2 = 1 \times 10^{-3}$) with relatively strong reaction, we observe a distinct delay in the onset of convection with increasing Da/Ra^2. At the same dimensionless time (ii), fingers in B, C, and D have only respectively grown by $\approx 4/5$, $\approx 4/5$, and $\approx 1/3$ of the depth of those in A, indicating slower finger growth rate as Da/Ra^2 increases. Note that C, with Ra higher than but Da/Ra^2 equal to that of B, exhibits finger growth rate similar to those of the latter. In all four cases at early times (i), an identical number of diffusive fingers $n \approx 56$ are seen sinking individually across the same dimensionless width $L_X/L_C = 7.5 \times 10^3$, revealing no change in the dimensionless wavelength of the instability $\lambda' = L_X/(L_C n)$. This observation is general for all simulations in the range explored and $\lambda' \approx 1.3 \times 10^2$, corresponding to a dimensionless wave number of $1/\lambda' \approx 8 \times 10^{-3}$, which is in agreement with previous numerical work for systems without chemical reaction [24].

B. Finger interaction

While the diffusive fingers initially propagate without interaction, the effect of Da/Ra^2 on finger interaction is clearly seen at later times. At time (iii), fingers in A, B, and C already show significant merging, thus becoming wider but fewer. The occurrence of these strong finger interactions in relatively high-Ra cases where reaction is also present, such as shown

in B and C, corroborates and complements previous studies based on nonreactive media [13]. Similar to A, the merged fingers of B and C at (iii) lengthen and continue to access the CO_2-rich solution at distinct "feeding sites" at the top, forming preferred pathways down which the CO_2 flows into the brine. The location and depth of the CO_2 pathways have been observed to shift with time, so that newly merged feeding sites form and elongate as previous ones diminish, sometimes in fluctuating, irregular cycles. In some cases, these larger, merged fingers may also at times split into several "branches" at the tip, before one of the branches dominates the others as the chosen pathway.

However, while strong finger interactions occur in inert and low Da/Ra^2 systems, for cases with higher Da/Ra^2 such as D, the finger interactions are significantly affected by the presence of reaction. Even at time (iii), a strong reaction in D inhibits the growth and merger of fingers and suppresses fluctuations in finger depth. As such, the CO_2 penetration depth reaches a maximum, and the length of the fingers is approximately uniform.

C. CO_2 mass flux dissolving at the top boundary

In Fig. 3, we plot the evolution of the CO_2 mass flux at the top boundary, for a range of values of Da/Ra^2. As Da/Ra^2 increases, the initial J' values become larger, suggestive of higher CO_2 dissolution rates from early times as faster, stronger reactions consume more of the CO_2 as it enters the system. Furthermore, the mass flux curves tend to flatten with increasing Da/Ra^2 as the effects of reaction steadily compensate for the decreasing flux due to diffusion, causing J' to deviate from an otherwise diffusive $-1/2$ slope and resulting in a less-pronounced minimum for J'. With increasing Da/Ra^2, the system enters the convective regime (i.e., when the flux rises from its minimum) at longer times, and J' rises with increasingly smaller slopes. Above a value of $Da/Ra^2 \approx 2 \times 10^{-3}$, reaction is strong enough to stabilize the system and prevent convection from altogether occurring. As previously discussed, the presence of strong reaction inhibits the formation of larger, merged fingers which may otherwise increase dissolution rates by channeling CO_2 downward. Instead, reaction favors smaller fingers with roughly uniform lengths, resulting in mass flux values which become steadier and more constant with increasing Da/Ra^2. When $Da/Ra^2 \approx$ O(1), reaction dominates both diffusion and convection: The CO_2 is consumed instantaneously as it enters the aqueous solution, leading to a constant inward flux without a boundary layer.

In Fig. 3, we also note that for cases B and C, which both have $Da/Ra^2 = 1.5 \times 10^{-4}$ but different individual Da and Ra values, the J' vs t' curves overlap before and at the onset of convection. These curves remain very similar even after the onset of instability, and the small discrepancies between them are likely due to numerical errors. Such overlap for cases B and C shows equal kinetic and fluid dynamic interactions in these cases, and that the group Da/Ra^2 completely governs the onset of convection in the presence of chemical reaction.

D. Time for onset of convection

From Fig. 3, we are also able to determine the time for onset of convection, t'_{oc}. Following Ref. [17], we define t'_{oc}

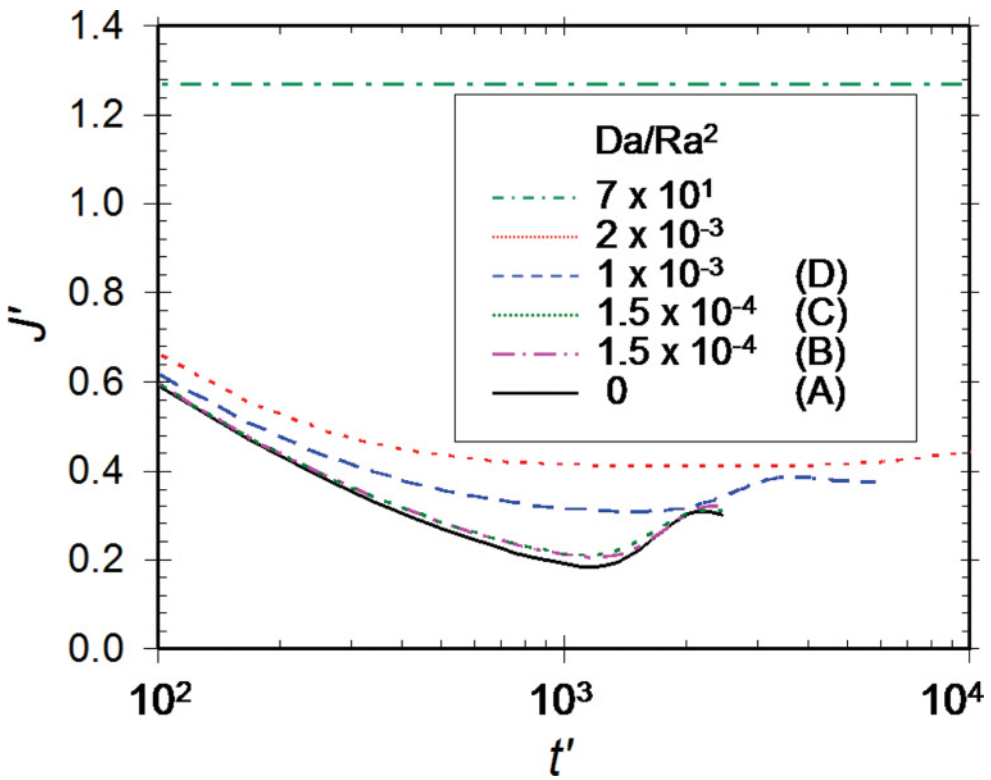

FIG. 3. (Color online) Evolution of CO_2 mass flux $J' = JL_C/(D\phi C_S)$ dissolving at the top boundary for selected Da/Ra^2, where $t' = tD/L_C^2$. Dimensionless time for onset of convection t'_{oc} corresponds to t' at minimum J'. Cases A–D refer to those shown in Fig. 2.

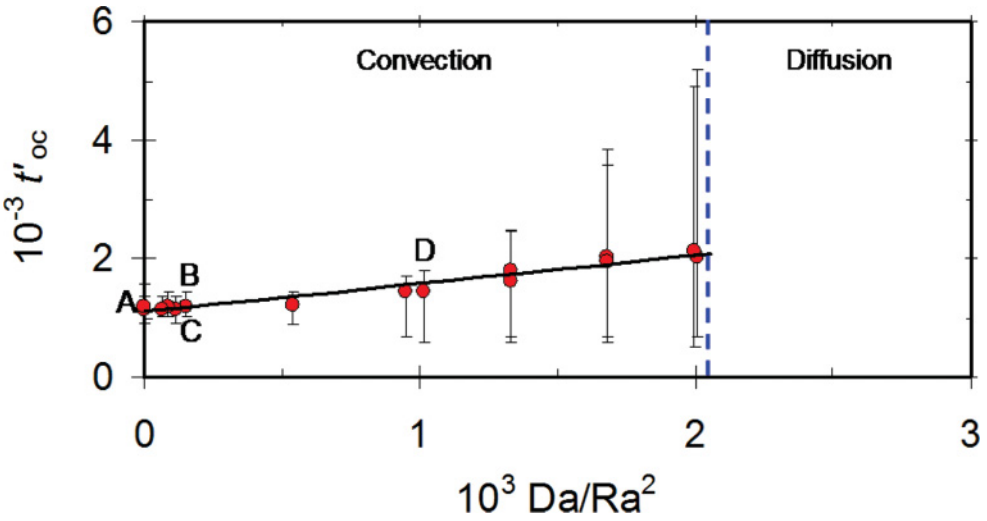

FIG. 4. (Color online) Dimensionless time for onset of convection t'_{oc} increases with Da/Ra^2 until $Da/Ra^2 \approx 2 \times 10^{-3}$ (blue dashed line), above which convection no longer occurs. Y-error bars reflect the error in locating the minimum value of J' in the curves in Fig. 3, i.e., flatter J' curves bring about larger error bars. Results of cases A–D (from Fig. 2) are shown.

as the time corresponding to the minimum J', the point at which the flux transitions from the diffusive to the convective regime. In Fig. 4, we show that the time for onset of instability t'_{oc} as a function of Da/Ra^2 is well described by $t'_{oc} = 1.1 \times 10^3 + 4.8 \times 10^5 Da/Ra^2$ for $Da/Ra^2 < 2 \times 10^{-3}$. As Da/Ra^2 increases, t'_{oc} becomes larger, resulting in a clear delay on onset of convection as the reaction becomes faster. The increasing Y-error bars reflect the error in identifying the minimum value of J' in the curves in Fig. 3. For inert systems ($Da/Ra^2 \approx 0$), $t'_{oc} \approx 1.1 \times 10^3$, which is in agreement with previous numerical work [24,25]. t'_{oc} for cases A, B, C, and D are also identified in Fig. 4, where for both B and C, $t'_{oc} \approx 1.2 \times 10^3$, which further indicates that the group Da/Ra^2 indeed completely governs flow and transport, independent of the individual values of Ra and Da. Above $Da/Ra^2 \approx 2 \times 10^{-3}$, reaction and diffusion dominate and convection no longer takes place.

IV. SUMMARY AND CONCLUSIONS

In this study, we have demonstrated that the stability of a buoyant boundary layer in a porous medium with a first-order chemical reaction is fully determined by the nondimensional number $Da/Ra^2 = k_r a D \phi \mu^2/(k \Delta \rho_0 g)^2$. This parameter is a measure of the rate of diffusion and reaction compared to convection. For low Da/Ra^2, the boundary layer breaks up into fingers which subsequently grow and merge, driving convection in the underlying fluid. As Da/Ra^2 increases, the growth rate of the instability decreases, the time for onset of convection increases, and finger interaction is delayed and suppressed. The dimensionless wavelength at the onset of instability does not depend on the presence of reaction. Above a critical value of $Da/Ra^2 \approx 2 \times 10^{-3}$, reaction stabilizes the planar diffusive layer at a finite depth and no convection develops in the fluid below. The depth of this stable diffusive layer decreases with increasing Da/Ra^2 until it approaches zero thickness at $Da/Ra^2 \approx O(1)$.

These results suggest that several regimes of transport of CO_2 stored in saline aquifers may occur, depending on how strongly aqueous CO_2 reacts with the porous rock. In weakly reactive systems, transport of CO_2 will occur throughout the whole depth of the reservoir, but with stronger reactions, the deeper part of the reservoir will be inactive.

Among deep saline reservoirs, the reaction strength can vary significantly. Rock matrices naturally possess a wide range of geochemical reaction rates depending on the mineralogy [16]. But even within the same mineralogy, approximations of overall geochemical rates, which take into account many factors affecting reaction strength, have been found to considerably vary, by up to several orders of magnitude [26]. In engineering applications, the reaction rate can be altered by changing the local temperature or the concentration of an active species in the rock matrix. Furthermore, there currently exists the technology to create and inject compounds to match specific reservoir requirements, and so, altering the strength of reaction by injecting a well-chosen reagent into a saline aquifer is possible.

ACKNOWLEDGMENT

J.T.H.A. gratefully acknowledges the Schlumberger Foundation for financial support.

[1] C. W. Horton and F. T. J. Rogers, J. Appl. Phys. **16**, 367 (1945).
[2] E. R. Lapwood, Math. Proc. Cambridge **44**, 508 (1948).
[3] Y. Katto and T. Masuoka, Int. J. Heat Mass Transfer **10**, 297 (1967).
[4] A. De Wit, Phys. Rev. Lett. **87**, 054502 (2001).
[5] A. De Wit, Phys. Fluids **16**, 163 (2004).
[6] C. Almarcha, P. M. J. Trevelyan, P. Grosfils, and A. DeWit, Phys. Rev. Lett. **104**, 044501 (2010).
[7] A. Postelnicu, Int. J. Heat Mass Transfer **52**, 2466 (2009).

[8] W. Kordylewski and Z. Krajewski, Chem. Eng. Sci. **39**, 610 (1984).
[9] H. Viljoen and V. Hlavacek, AIChE J. **33**, 1344 (1987).
[10] W. W. Farr *et al*., AIChE J. **37**, 963 (1991).
[11] M. S. Malashetty, P. Cheng, and B. H. Chao, Int. J. Heat Mass Transfer **37**, 2901 (1994).
[12] *IPCC Special Report on Carbon Dioxide Capture and Storage*, edited by B. Metz *et al*. (Cambridge University Press, Cambridge, UK, 2005).
[13] A. Riaz *et al*., J. Fluid Mech. **548**, 87 (2006).
[14] E. Lindeberg and P. Bergmo, in *The 6th International Conference on Greenhouse Gas Control Technologies*, edited by J. Gale and Y. Kaya (Elsevier Science, Amsterdam, 2003).
[15] J. Ennis-King and L. Paterson, SPE J. **10**, 349 (2005).
[16] J. Ennis-King and L. Paterson, in *The 8th International Conference on Greenhouse Gas Control Technologies*, edited by J. Gale and O. Bolland (Elsevier, Oxford, 2007).
[17] J. J. Hidalgo and J. Carrera, J. Fluid Mech. **640**, 441 (2009).
[18] E. Holzbecher, *Modeling Density-Driven Flow in Porous Media* (Springer, New York, 1998).
[19] D. A. S. Rees, A. Selim, and J. P. Ennis-King, in *Emerging Topics in Heat and Mass Transfer in Porous Media From Bioengineering and Microelectronics to Nanotechnology*, edited by P. Vadasz (Springer, The Netherlands, 2008).
[20] CSIRO, *Fastflo Tutorial Guide* (version 3) (CSIRO, Australia, 2000).
[21] J. W. Elder, J. Fluid Mech. **27**, 609 (1967).
[22] C. I. Voss and W. R. Souza, Water Resour. Res. **23**, 1851 (1987).
[23] M. J. Simpson and T. P. Clement, Adv. Water Resour. **26**, 17 (2003).
[24] H. Hassanzadeh, M. Pooladi-Darvish, and D. W. Keith, AIChE J. **53**, 1121 (2007).
[25] H. Hassanzadeh, M. Pooladi-Darvish, and D. W. Keith, Transp. Porous Med. **65**, 193 (2006).
[26] O. M. Phillips, *Geological Fluid Dynamics: Sub-surface Flow and Reactions* (Cambridge University Press, Cambridge, UK, 2009).